

Relevance of Ventricular Electrical Dispersion to Arrhythmogenesis in Ischemic Myocardium – A Simulation Study

H. ZHANG^{1,2}, Z. X. ZHANG¹, L. YANG³, Y. B. JIN^{1,2} AND Y. Z. HUANG¹

¹ *The Key Laboratory of Biomedical Information Engineering of the Ministry of Education of China, Institute of Biomedical Engineering, School of Life Science and Technology, Xi'an Jiaotong University, Xi'an, P. R. China. E-mail: maxr@263.net*

² *Electric Engineering and Electronics Teaching Experiment Center, Xi'an Jiaotong University, 710049 Xi'an, P. R. China*

³ *Cardiology Department, The First Hospital, Xi'an Jiaotong University, 710061 Xi'an, P. R. China*

Abstract. A computer simulation method was used to study the possible role of electrical dispersion induced by regional ischemia in the mechanisms underlying cardiac arrhythmias. Ischemic cells were simulated by considering the three major component conditions of acute ischemia (elevated extracellular K^+ concentration, acidosis and anoxia) at the level of ionic currents and ionic concentrations. An ischemic area was introduced into a homogeneous healthy tissue to create a localized inhomogeneity. The constructed models were solved using the operator splitting and adaptive time step methods. The numerical experiments showed that action potential durations (APDs) of ischemic cells did not change with beats of shorter or longer cycle length. The smaller percentage increase of slow component of the delayed rectifier K^+ current, I_{ks} , and smaller outward Na^+ - Ca^{2+} exchange current were found to be the ionic mechanisms underlying the decreased rate dependence in ischemic cells. The results suggest that ischemia flattens the APD restitution curve; however, the dispersion of refractory period can be greatly increased by a premature beat in the constructed inhomogeneous sheet. This demonstrates that the dispersion of refractoriness rather than APD by a premature beat contributes to reentrant tachyarrhythmias in the locally ischemic tissue.

Key words: Arrhythmia — Computer simulations — Ischemia — Reentries — Refractoriness

Correspondence to: Zhenxi Zhang, The Key Laboratory of Biomedical Information Engineering of the Ministry of Education of China, Institute of Biomedical Engineering, School of Life Science and Technology, Xi'an Jiaotong University, 28 West Xianning Road, 710049 Xi'an, P. R. China. E-mail: zxzhang@mail.xjtu.edu.cn

Introduction

Cardiac arrhythmias constitute a major clinical problem that presents itself in many ways, with the worst manifestation being sudden death. In many cases, the cause of death is ventricular tachycardia (VT) and its degeneration into ventricular fibrillation (VF). There is overwhelming experimental evidence suggesting that the underlying mechanism responsible for sustaining VT or VF is reentry, in which the wave of excitation, instead of propagating more or less rectilinearly, turns upon itself and “reenters” the same territory, re-exciting the tissue it has excited previously.

Reentry can be initiated even in normal and healthy hearts, but it is more common in hearts with structural and/or functional abnormalities such as ischemia. It has been suggested recently that spiral waves, a form of self-sustained reentrant activity that has been described in many excitable media, might be responsible for these arrhythmias (Winfree 1994; Cascio 2001).

In ischemic heart, blood flow to the heart muscle is reduced, starving it of oxygen and metabolites, and leading it to undergo complex and poorly understood biochemical and metabolic changes. The results are a decrease in overshoot potential and amplitude, shortening of action potential duration (APD), slowdown of upstroke velocity and conduction velocity, depolarization of resting potential (Clayton et al. 2002), and appearance of post-repolarization refractoriness (Carmeliet 1999).

To date, most simulation studies of arrhythmia during ischemia have been concentrating on investigating the effects of extracellular potassium accumulation alone (Aoxiang and Michael 1998; Xie et al. 2001). Other factors, such as ATP-regulated potassium current ($I_{K(ATP)}$), have not been considered, although the ischemia-induced action potential shortening, which could play an important role in electrical dispersion and reentry, might depend on activation of K_{ATP} channels (Noma 1983; Shaw and Rudy 1997a,b). To carry out a more realistic study, we simulated ischemic cells considering the three major component conditions of acute ischemia (elevated extracellular K^+ concentration $[K^+]_o$, acidosis and anoxia) at the level of ionic currents and ionic concentrations. Then, by introducing ischemic cells into a normal sheet of ventricular myocardium, spatially distributed electrical dispersion was constructed to study the effects of regional ischemia on arrhythmogenesis.

Materials and Methods

Selection of numerical model

We constructed an excitable medium model of a mammalian ventricular tissue by incorporating ordinary differential equations for ventricular cell excitability into a partial differential equation model for diffusion of the excitability. Thus, the fundamental decision to be taken upon embarking on studying reentry mechanisms was the choice of ionic model for ventricular cell excitability. Several mathematical

ionic models of ventricular muscle are available. They summarize the results of voltage clamp experiments – these include the Beeler–Reuter model (Beeler and Reuter 1977), the Phase 1 Luo-Rudy model (Luo and Rudy 1991), and the guinea-pig ventricular cell model specified by Noble et al. (1991, 1998), and the Phase 2 Luo-Rudy models (Luo and Rudy 1994). None of them is definitive in that they all represent steps in an ongoing process of modeling the behavior of ventricular cells. The Noble et al. (1991, 1998) and Luo and Rudy (1994) models have concentrations of several of the ionic species Na^+ , K^+ and Ca^{2+} that vary in time rather than stay fixed, internal Ca^{2+} dynamics (involving Ca^{2+} uptake by and release from sarcoplasmic reticulum), and Na^+ - K^+ pump and Na^+ - Ca^{2+} exchange currents. These detailed models are more realistic in reproducing the characteristics of the cellular electrophysiology.

The Noble models have so far been used in about twenty modeling studies (Biktashev and Holden 1998, 2002; Clayton et al. 2002). In this paper, we used the equations of Noble et al. (1991). However, the delayed rectifier K^+ current was replaced by the rapid (I_{kr}) and slow (I_{ks}) components described in Noble et al. (1998), and ATP-sensitive K^+ current was incorporated into the equations. $I_{K(\text{ATP})}$ is inactive in healthy ventricular tissue and is increasingly outward with aggravation of ischemia. The formula is

$$I_{K(\text{ATP})} = G_{K(\text{ATP})} \frac{V + 80}{1 + \left(\frac{[\text{ATP}]_i}{0.1} \right)^2} \quad (1)$$

where V is the transmembrane potential (mV), $[\text{ATP}]_i$ is the intracellular ATP concentration (mmol/l), $G_{K(\text{ATP})}$ is the maximum channel conductance *per* cell at 0 mol/l $[\text{ATP}]_i$.

Numerical methods

Ignoring the microscopic cell structure, cardiac tissue can be treated as a continuous system in which a two-dimensional sheet of isotropic ventricular muscle is modeled by a reaction-diffusion system as follows:

$$\frac{\partial V}{\partial t} = \frac{1}{C_m} (-I_{\text{ion}}) + D \left(\frac{\partial^2 V}{\partial x^2} + \frac{\partial^2 V}{\partial y^2} \right) \quad (2)$$

where D is the diffusion coefficient for transmembrane potential, C_m is the membrane capacitance, I_{ion} is the total ionic current, t is time, x and y are spatial coordinates in the sheet. Here we use of $D = 31.25 \text{ mm}^2/\text{s}$, which gives the conduction velocity for a normal solitary plane wave along one of the coordinate axes of about 400 mm/s. It was reported that the canine ventricular conduction velocities ranged from 140–250 mm/s (transverse) to 500–800 mm/s (longitudinal) (Biktashev and Holden 1998), so our value of D was in-between the longitudinal and transverse diffusion coefficients in a real anisotropic myocardium.

I_{ion} is a function of voltage V , gating variables $Y_1, \dots, Y_i, \dots, Y_M$, and of ion concentrations $Z_1, \dots, Z_i, \dots, Z_N$. In general, the gating variables Y_i satisfy ordinary differential equations (ODE) of the following type:

$$\frac{dY_i}{dt} = \alpha_i(1 - Y_i) - \beta_i Y_i \quad i = 1, \dots, M \quad (3)$$

where α_i are rate constants and depend β_i only on voltage. The ion concentrations Z_i satisfy another set of ODE:

$$\frac{dZ_i}{dt} = f_i(I_{Z_i}, V, Z_i) \quad i = 1, \dots, N \quad (4)$$

where I_{Z_i} is the ionic current related to Z_i .

Because of the stiffness of the partial differential Eq. (2), numerical integration using a conventional Euler method requires the time step to be very small during the action potential upstroke to keep numerical stability and accuracy. To improve the integration efficiency, an advanced algorithm (Jin et al. 2004) was used to integrate Eqs. (2–4). In Jin et al. (2004), we investigated the numerical algorithm suggested by Qu et al. (1999) for conduction of action potential in a two-dimensional cardiac tissue. The solving procedure was divided into two steps using a time splitting method. An adaptive time step method was applied to solve for action potential of individual cells. The alternating direction implicit (ADI) method or the five-point centered difference method was employed to integrate the partial differential equations (PDEs). Our results showed that when the time splitting and adaptive time step methods were adopted, the integration accuracy of the PDEs using the ADI method was slightly higher compared to the five-point difference method, but the computation time of the latter method was by 30% shorter. Therefore, we integrated Eq. (2) as follows:

Step 1. Use the result at time t as an initial condition to integrate the following PDE over a time step of $\Delta t/2$:

$$\frac{\partial V}{\partial t} = D \left(\frac{\partial^2 V}{\partial x^2} + \frac{\partial^2 V}{\partial y^2} \right) \quad (5)$$

Step 2. Use the result of Step 1 as the initial condition to integrate the following ODE with Eq. (3) and Eq. (4) over a time step of Δt :

$$\frac{dV}{dt} = \frac{1}{C_m} (-I_{\text{ion}}) \quad (6)$$

Step 3. Use the result of Step 2 as the initial condition to integrate the PDE Eq. (5) again over a time step of $\Delta t/2$.

In practice, Step 1 and Step 3 may be combined into a single step, except for the first and the last step of the whole time interval of integration.

To solve Eq. (5) numerically, we used a five-point centered difference method with impermeable boundary conditions:

$$\left. \frac{\partial V}{\partial x} \right|_{x=x_{\min}, x_{\max}} = \left. \frac{\partial V}{\partial y} \right|_{y=y_{\min}, y_{\max}} = 0 \quad (7)$$

The time step $\Delta t = 0.05$ ms was used to keep all cells synchronized. The spatial step was $\Delta x = \Delta y = 0.01$ cm.

We integrated Eq. (6) using a second-order Runge-Kutta method with adaptive time step that was varied between a minimum ($\Delta t_{\min} = 0.01$ ms) and a maximum time step ($\Delta t_{\max} = 0.05$ ms).

Compared with the conventional Euler method, this approach speeds up the integration about 6-fold, with relative error not exceeding 2%.

The numerical integration was run on a personal computer with a 2.8 GHz processor. All programs were written in Visual C²⁺.

Simulation of myocardial ischemia

Numerical experiments were conducted in a two-dimensional sheet with 100×100 elements. The length of each element was $100 \mu\text{m}$, so that the thin-sliced square section of the ventricular myocardium corresponded to 10×10 mm. Each element was considered a cluster of homogeneous myocardial cells, and was electrically coupled with four immediate neighbors by gap junctions.

A simulated local ischemia was introduced into the “healthy” sheet. The physical size and shape of the ischemic region could be changed during the study, but electrophysiological properties of cells in a specific ischemic zone were assumed uniform.

To produce different spatial heterogeneity, two ischemic models were developed by changing physiological variables in a selected area. The ionic and metabolic conditions of acute ischemia that affect cell electrophysiology were introduced as three

Table 1. Properties of the simulated normal, moderately ischemic, and severely ischemic cells

	$[\text{K}^+]_o$	Anoxia	Acidosis		Measured parameters			
	$[\text{K}^+]_o$ (mmol/l)	$[\text{ATP}]_i$ (mmol/l)	G_{Na} (μS)	G_{CaL} (μS)	APD ₉₀ (ms)	V_{max} (V/s)	Resting potential (mV)	Post-repolarization refractoriness (ms)
Normal	4.5	8.0	2.5	0.25	152	381	-89	-9
Moderate ischemia	8.5	3.0	1.75	0.20	75	249	-73	71
Severe ischemia	10.5	1.0	1.0	0.14	50	151	-67	113

components: i) an increase in $[K^+]_o$, ii) intracellular and extracellular acidosis (decrease in pH), and iii) anoxia and metabolic blockade (decrease in $[ATP]_i$). It has been reported that extracellular acidosis reduces availability of I_{Na} , and intracellular acidosis reduces availability of I_{CaL} (Shaw and Rudy 1997a,b). Therefore, in our models the maximum conductances (G_{Na} and G_{CaL}) of I_{Na} and I_{CaL} were decreased to simulate ischemic acidosis. Direct electrophysiological effects of anoxia were modeled by introducing $I_{K(ATP)}$. Computational models of moderate and severe ischemia were constructed. The parameters and properties of these models are shown in Table 1.

Results

Physiological behavior of simulated ischemic cells

Some important electrophysiological parameters were measured by exerting a 10-beat drive train on a simulated single cell. Each stimulus was $12 \mu A/\mu F$ in amplitude and 2 ms in duration (the stimuli used in our numerical experiments were the same unless otherwise stated). Cycle length of the stimuli was 1000 ms. APD_{90} (the time it takes a cell to repolarize to 90% of its resting potential), resting potential and \dot{v}_{max} (the maximum membrane rate of depolarization) were measured. Moreover, post-repolarization refractoriness was determined by the extrastimulus technique. After a train of eight regular stimuli S1 with a cycle length of 1000 ms, an early “ineffective” extrastimulus S2 was introduced. During consecutive stimulation cycles, the extrastimulus was introduced progressively later until it triggered an action potential. The interval between the latest S1 and S2 is the S1–S2 interval. Post-repolarization refractoriness is defined as the difference between the S1–S2 interval and APD_{90} .

Data in Table 1 and Fig. 1A demonstrate that the simulated ischemic cell is characterized by an obvious reduction in APD, slower APD upstroke, and less negative resting potential, just as observed in experiment (Carmeliet 1999). Moreover, ischemic cells display the property of post-repolarization refractoriness. During ischemia the refractory period prolongs, despite shortening of the APD, and outlasts full repolarization by tens or even over one hundred milliseconds.

In general, a cardiac membrane normally recovers excitability on the tail of a preceding action potential and full excitability begins with return to resting potential. Ischemia delays the recovery of excitability beyond the return to resting potential. Fig. 1B shows the sodium channel inactivation gating variable h , which provides the degree of I_{Na} recovery and the fraction of available sodium channels. Gate h is 99% recovered after 38 ms in normal cells, but only 71% after 167 ms and 41% after 189 ms in moderately and severely ischemic cells, respectively. This illustrates that gate h is smaller in ischemic cells and needs a longer recovery time. With higher level of ischemia, it further decreases and needs a much longer recovery time, which results in lower excitability and longer refractory period.

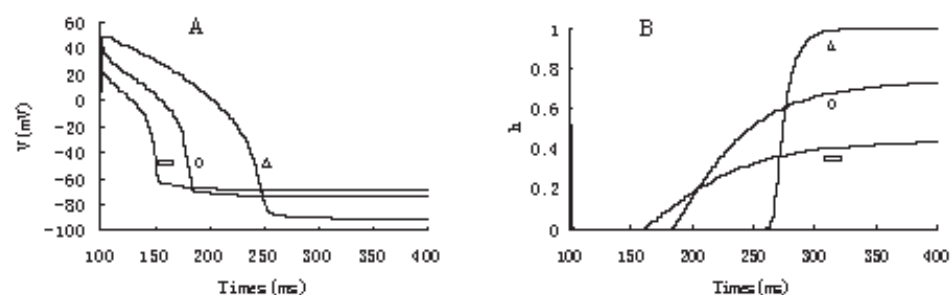


Figure 1. Action potentials (Panel A) and corresponding sodium channel inactivation gate h (Panel B) of the simulated normal (Δ), moderately (\circ) and severely ischemic (\square) cells.

Characteristics of the constructed locally ischemic tissue

One of the specific distributions of regional ischemia in our study is shown in Fig. 2A. The two-dimensional sheet includes 100×100 elements. Normal cells are located on the border of the sheet indicated by darker color. The moderately or severely ischemic cells as defined in Table 1 are placed in the area indicated by lighter gray. A thin stripe of ischemic tissue extends to the border of the sheet.

A train of 10 current pulses S1 was applied on the tissue to the upper right corner area of 0.5×0.5 mm. The basic cycle lengths (BCLs) of the S1 stimuli were 200, 600, and 1000 ms.

Fig. 2B shows the depolarizing and repolarizing processes for different levels of ischemia at different BCLs after the 10th stimulus S1 is applied.

In Fig. 2B (1), the severely ischemic area is clearly visible within the sheet because the resting potential is depolarized to about -67 mV as a consequence of $[K^+]_o$ being set to 10.5 mmol/l in that area. In the moderate case, the ischemic area is not so obvious since $[K^+]_o$ is just 8.5 mmol/l, which leads to resting potential of 73 mV.

In severe ischemia, the depolarizing processes at different BCLs are similar. There are obvious delays in action potential waves propagating in ischemic regions that make wave fronts curve distinctively. However, the effect is less evident in the moderately ischemic condition due to the larger APD upstroke and faster velocity.

In contrast, repolarizing processes exhibit different characteristics at different BCLs in the conditions of severe local ischemia. The normal area at the same position repolarizes earlier at shorter BCL (e.g., Fig. 2B (1)) than it does at longer BCL (e.g., Fig. 2B (3)). Thus, in frames J, while all normal cells have returned to the resting potential at BCL = 200 ms, there are still normal areas (such as cells at the bottom), which have not completely repolarized at BCL = 600 ms. The phenomenon is even more evident at BCL = 1000 ms. The same effect can be seen also in the moderate ischemia condition. It illustrates that there is a rate-dependent characteristic of repolarization of normal cells.

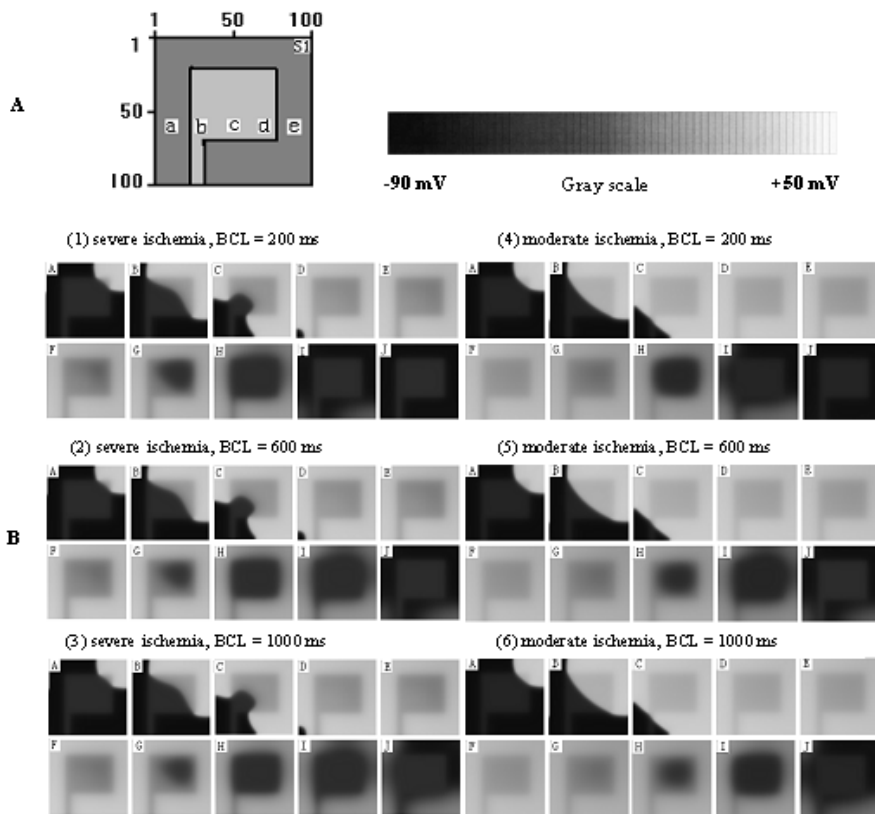


Figure 2. Depolarizing and repolarizing processes in severe and moderate ischemia at different BCLs. **A.** Spatial ischemic region of the simulated inhomogeneous sheet. The darker area represents normal tissue. The ischemic region is in lighter color. S1 denotes the stimulus position. Action potentials are recorded at sites a (10, 60), b (23, 60), c (50, 60), d (77, 60) and e (90, 60) in the matrix. **B.** Frames show the depolarizing and repolarizing processes after the start of stimulation S1. The activation waves (frames A to E) are displayed every 10 ms. The repolarizing processes (frames F to J) are recorded every 20 ms. The gray scale gives transmembrane potential of the frames A to J.

After inspecting Fig. 2B we find that the ischemic regions display similar repolarizing processes regardless of the BCL, so they manifest a rate-independent property. This indicates that relevance of the APD to BCL for normal cells is very different from that of ischemic cells.

Fig. 3A shows action potentials recorded at different BCLs in the severely ischemic case. Unlike action potentials at normal sites a and e, action potentials at sites b, c and d exhibit the properties of less negative resting potential, smaller amplitude and shorter duration. The results are in good agreement with the data

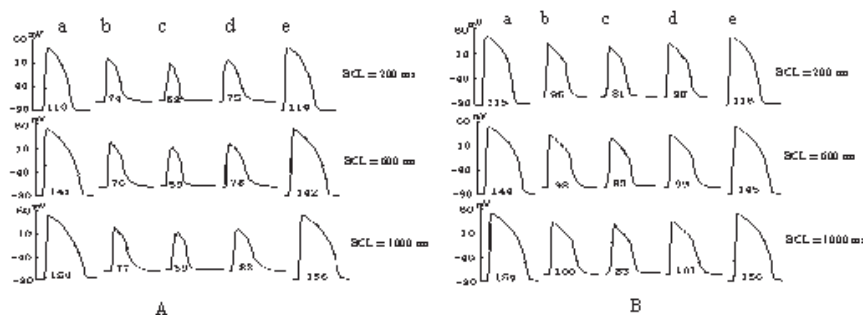


Figure 3. Action potentials at sites a, b, c, d and e in the severely (Panel A) and moderately (Panel B) ischemic tissue, respectively. APD (in ms) is indicated under each action potential.

in Table 1. However, compared with APDs at site c, APDs at sites b and d at the three BCLs are prolonged, though the physiological parameters are the same at the three sites in simulation. This illustrates that an electrotonic interaction occurs, which makes the APDs show a spatially homogenizing effect near the border zone between the normal and ischemic area. The above phenomena can also be observed in Fig. 3B, though APDs at sites b, c, and d are a little longer because of the less severe ischemia.

In Fig. 3, when beats of shorter or longer cycle length are interposed, the overall effect in normal elements (e.g., at site a, APD = 110 ms at BCL = 200 ms, APD = 154 ms at BCL = 1000 ms) is shortening of APDs after shorter intervals and lengthening of APDs after longer intervals. This closely resembles the characteristics seen in Fig. 2. In other words, for normal elements, the rate-dependent characteristic is remarkable. However, this kind of dependence is absent in ischemic elements. The APDs remain almost constant at site c at different BCLs. The phenomenon has been observed in experiment (Taggart et al. 1996), but the mechanisms have not yet been fully investigated by now.

The ability of cardiac myocytes to adjust their APDs to changes in pacing frequency is termed adaptation (Viswanathan et al. 1999). Under normal conditions, the most prominent effect of decreasing BCL is shortening of APD. To investigate the underlying ionic mechanisms of APD adaptation, we examined some transmembrane currents (I_{kr} , I_{ks} , I_{CaL} , and I_{NaCa}) that could play an important role during the plateau and repolarization phases of the action potential. Fig. 4 summarizes action potentials and currents under the normal and severely ischemic conditions at rapid (BCL = 200 ms) and slow pacing (BCL = 1000 ms). Upstrokes of the action potentials are aligned to facilitate comparison.

The results of Fig. 4 provide some insight into the processes that underlie adaptation. In normal or ischemic cells, I_{kr} (Fig. 4B) is similar at the two frequencies (differences secondary to APD difference should not be considered and

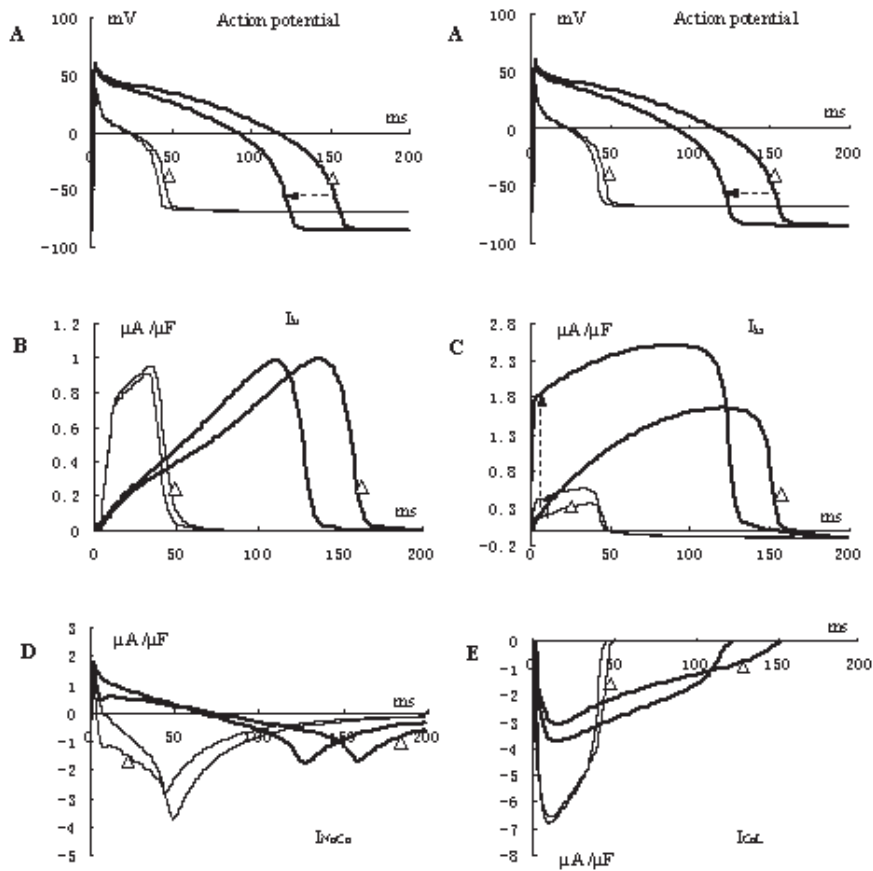


Figure 4. Mechanisms of rate dependence in the normal cell and decreased adaptability of the ischemic cell. Computed action potentials (Panel A), rapid (I_{kr} , Panel B) and slow (I_{ks} , Panel C) components of the delayed rectifier K^+ currents, Na^+ - Ca^{2+} exchange currents (I_{NaCa} , Panel D) and L-type calcium currents (I_{CaL} , Panel E) of the normal (bold line) and severe ischemic (thin line) cell at slow (with symbol Δ , BCL = 1000 ms) and fast (without symbol, BCL = 200 ms) rates are summarized.

currents should be compared at the same V), which reflects its smaller effect on rate adaptation. However, the arrows in Fig. 4C show that there is a greater residual activation of I_{ks} for the shorter BCL at the onset of depolarization of a normal cell, which results in the greater repolarization current.

At short BCL, I_{NaCa} (Fig. 4D) is initially a remarkably outward current during the plateau phase of the action potential. This is due to the accumulation of intracellular ionic Ca^{2+} and Na^+ concentration. The increased outward I_{NaCa} acts to shorten APD at shorter BCL. However, this current diminishes relatively quickly,

reverses direction, and becomes a relatively large depolarizing current. This limits the role of I_{NaCa} in APD shortening.

I_{CaL} (Fig. 4E) exhibits a little larger plateau magnitude at short BCL. As the I_{CaL} is an inward current, this would act to prolong the APD rather than shorten it, so this current cannot contribute to APD shortening.

This implies that adaptation processes under normal conditions are due to the accumulation of I_{ks} activation caused by incomplete deactivation, together with the initially increased outward current I_{NaCa} that acts to shorten the APD at the shorter BCL.

The important information in Fig. 4 can also explain the less distinct adaptability of ischemic cells. Obviously, there is a smaller percentage increase of I_{ks} in a severely ischemic cell (96%, compared with 390% in normal cells) with BCL shortening, which accounts for the decrease in adaptability. Moreover, in contrast with normal cells, at the onset of depolarization I_{NaCa} in ischemic cells shows a less pronounced outward feature at the shorter BCL and the current reverses much more quickly and becomes a larger depolarizing current. So the smaller increase in currents I_{ks} and I_{NaCa} may contribute to the smaller shortening in APD at the shorter BCL, which underlies the much smaller rate-dependence of ischemic cells.

From Fig. 4E, we can also note that I_{CaL} increases in ischemic conditions, in spite of acidic depression of G_{CaL} (Shaw and Rudy 1997a,b). In contrast to normal cells, the inward Na^+ current becomes much smaller in ischemic state, which makes the contribution of the I_{CaL} current to cell depolarization relatively greater. I_{CaL} is a slowly activated current and, therefore, with the depressed Na^+ current it leads to the smaller upstroke velocity of the action potential during ischemia.

APD restitution and dispersion of refractory period

The above findings illustrate that normal and ischemic cells exhibit many different properties in action potentials. It is reported that dispersion of APD enhances arrhythmogenesis by reentrant mechanisms, and APD may have a significant effect on a reentrant circuit (Tsunetoyo et al. 2000; Starmer et al. 1995). To determine the main cause of reentry, we measured interval dependence of the APD, which is often referred to as the electrical restitution curve, at sites a (normal cell) and c (severely ischemic cell).

APD restitution was determined by delivering eight consecutive stimuli S1 to a 0.5×0.5 mm area in the upper right corner, with a coupling interval of 1000 ms, followed by an S2 stimulus to the same position. APD_{90} of the S2 were then measured at sites a and c, and plotted as a function of the S1–S2 coupling interval (interval between the latest S1 and S2) in Fig. 5.

Fig. 5 suggests that ischemia flattens electrical restitution of APD, and the difference in APD between normal and ischemic cells decreases with shortening of the S1–S2 interval.

Fig. 6 is the measured interval dependence of the effective refractory period (ERP) at sites a and c. It was determined by exerting an S1–S2–S3 stimulus. After a train of eight regular stimuli S1 with a cycle length of 1000 ms, a stimulus S2 was

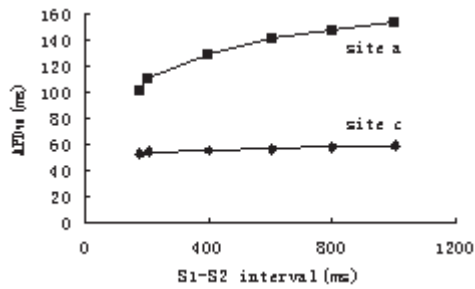


Figure 5. Action potential duration (APD) restitution curves at site c (severe ischemia) and site a (normal tissue).

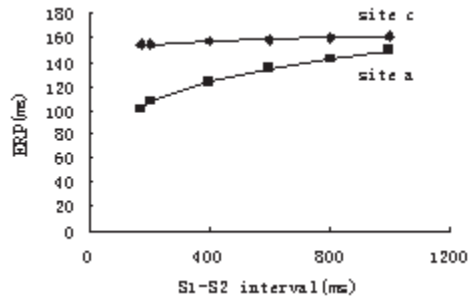


Figure 6. Relation between the S1-S2 interval and effective refractory period (ERP) at sites a and c, respectively.

applied. Then an early “ineffective” extrastimulus S3 was introduced progressively later until it could trigger an action potential. The interval between the latest S1 and S2 was defined as the S1-S2 interval. The duration between S2 and S3 was the ERP.

Fig. 6 shows that the refractory period of a normal cell decreases with shortening of the stimulus interval, but for a severely ischemic cell, the refractory period remains almost constant. Thus, a decrease in the stimulus interval can result in greater dispersion of refractory period. This indicates that a premature beat may increase overall dispersion of refractoriness in a locally ischemic tissue.

Spiral waves induced by a premature beat

Fig. 7 displays a spiral wave initiated by a premature beat in ischemic tissue. After applying a train of eight stimuli S1 to the upper right corner area of 0.5×0.5 mm, a premature stimulus S2 was applied to the bottom left corner of the simulated sheet. To save computation time, the BCL of the S1 stimulus was 400 ms. The interval between the latest S1 and the premature stimulus was 120 ms.

At the beginning of the premature stimulus S2, the simulated ischemic tissue is still refractory due to the post-repolarization refractoriness, even though it has

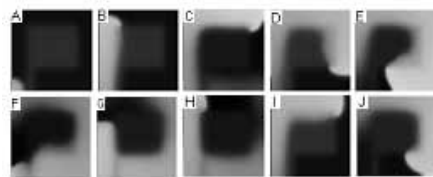


Figure 7. Initiating process of a spiral wave in the two-dimensional simulated tissue. Frames are recorded every 20 ms after the start of stimulation S2.

returned to the resting potential. The impulse wave is blocked by the extended ischemic part, but it can successfully propagate in the clockwise direction along the normal tissue that has already repolarized (frames A to E). Because the extended part of the ischemic area is very small and its excitability has recovered by the time the wavefront reached this region, the large source current can activate and penetrate this area (frame F) and continue to propagate along the boundary to form a reentrant wave (frames G to J).

Two kinds of sustained spiral wave patterns have been observed in our study. One occurs in the moderately ischemic situation. When excitability of ischemic cells has recovered, the wavefront can activate this area. When ischemic cells become unexcitable due to their longer refractory periods, the wave tends to move along the sharp border between the normal and ischemic tissues until excitability of ischemic cells recovers again. Therefore, the tip of the spiral wave meanders on a large circuit with fast velocity, which leads to reentrant excitation characterized by unstable functional reentrant circuits. Another type of spiral waves occurs in severe myocardial ischemia with low excitability. The conduction velocity reduces by more than a half compared to the value in normal myocardium due to reduced action potential amplitude and upstroke velocity. Thus, the spiral wave is almost completely blocked by the ischemic area and tends to move along the border between the normal and ischemic tissues. The tip of the spiral wave is anchored to the border, which results in a more stable reentry with significantly slower speed than the waves in regions with moderate ischemia. The occurrence of the two kinds of spiral waves indicates that in myocardial ischemia, the condition disturbances are mainly determined by the development of inexcitability at the cellular level.

Discussion

A ionic model based on myocardial ionic dynamics was used in our simulation study. The model could better approximate the real dynamics of myocardial ionic currents and thus achieve higher accuracy in studying the mechanisms of cardiac arrhythmias. The shapes and properties of action potentials in our simulated ischemic models were in good agreement with other studies (Clayton et al. 2002; Shaw and Rudy 1997a).

The simulation shows that in ischemic cells K^+ accumulation outside the cell has major effect on cell excitability by depolarizing the resting membrane potential and causing reduction in sodium channel availability. Post-repolarization refractoriness of the APD results from the delayed recovery of excitability. Decrease of the $[ATP]_i$ concentration leads to obvious reduction in APD. Conduction velocity is markedly slowed down by the ischemic area. These results are consistent with experiment (Carmeliet 1999).

Ischemic cells display rate-independent characteristics. The smaller increases in currents I_{ks} and I_{NaCa} at the onset of depolarization at short BCLs are found to be the underlying ionic mechanisms. Moreover, I_{CaL} increases during ischemic

conditions, although acidosis is proved to depress conductance of the calcium current in this case (Irisawa and Sato 1986; Shaw and Rudy 1997a). This reflects an increased driving force during the lower plateau of the ischemic action potential.

It has been reported that reentry occurrence in ischemic hearts is relatively higher than in normal hearts. Our simulation indicates that APD and refractory period of ischemic cells change very little with decrease of BCL of stimulus, thus leading to flattening of the APD restitution curve. Dispersion of APD reduces with BCL shortening in a locally ischemic tissue. These results seem to contradict the suggestions of Qu et al. (1999, 2000), who show that the converse, steepening of the restitution curve, is proarrhythmic or leads to "chaos". They point out that steepening of restitution breaks spiral waves (reentry) into smaller ones, the spiral breakup being the equivalent of fibrillation. One could therefore argue that flattening of the APD restitution curve is protective. Yet, recently, Wu and Lim (2002) and Chen et al. (2003) have used optical mapping techniques to study Langendorff-perfused rabbit heart. They found two types of VF in isolated rabbit hearts. Type I (fast) VF is associated with steep APD restitution and normal excitability. Type II (slow) VF is associated with flat APD restitution and decreased excitability. We therefore suggest that acute regional ischemia preceding the onset of VF could depress excitability sufficiently to produce immediate type II VF in the ischemic zone.

We demonstrate that, compared with the APD during ischemic conditions, the overall refractory period is prolonged due to the long recovery time of excitability. The presence of post-repolarization refractoriness makes refractory period outlast APD by as much as over one hundred milliseconds. The dispersion of refractory period between normal and ischemic regions is greatly increased with BCL shortening, although the dispersion of APD decreases.

In summary, we suggest that the dispersion of refractoriness, rather than of APD, contributes to reentrant tachyarrhythmias. Moreover, premature beats can strengthen this dispersion. We propose that this is the principal mechanism whereby the ventricular tachycardia in patients with coronary heart disease is easily initiated by a premature beat and leads to reentry (Janse 1992).

The computational cell model that we used in this study is relatively simple, as it does not include detailed simulation of hypoxia and acidosis associated with ischemia. Yet the relative computational simplicity enables simulation of action potential propagation in an extended tissue. The movement of reentry source along a sharp inhomogeneity is consistent with the results of experimental mapping of rabbit ventricular wall (Fast and Pertsov 1992).

Although other factors, including the three-dimensional geometry and anisotropy of conduction in real myocardium, undoubtedly play a role in the genesis of VT and VF, we suggest that electrical dispersion in refractoriness is most probably a fundamental mechanism of ischemia-related arrhythmias in locally ischemic tissues.

Acknowledgements. This study was supported by the National Natural Science Foundation of the P. R. China (No. 60378018 and 30100067) and the Doctoral Foundation of Xi'an Jiaotong University DFXJTU 2003-12, P. R. China.

References

- Aoxiang X., Michael R. G. (1998): Two forms of spiral-wave reentry in an ionic model of ischemic ventricular myocardium. *Chaos* **8**, 157—175
- Beeler G. W., Reuter H. (1977): Reconstruction of the action potential of ventricular myocardial fibres. *J. Physiol. (London)* **268**, 177—210
- Biktashev V. N., Holden A. V. (1998): Re-entrant waves and their elimination in a model of mammalian ventricular tissue. *Chaos* **8**, 48—56
- Biktashev V. N., Holden A. V., Mironov S. F., Pertsov A. M., Zaitsev A. V. (2002): Three dimensional organization of re-entrant propagation during experimental ventricular fibrillation. *Chaos Soliton Fractals* **13**, 1713—1733
- Carmeliet E. (1999): Cardiac ionic currents and acute ischemia: from channels to arrhythmias. *Physiol. Rev* **79**, 917—1017.
- Cascio W.E. (2001): Myocardial ischemia: what factors determine arrhythmogenesis? *J. Cardiovasc. Electrophysiol.* **12**, 726—729
- Chen P. S., Wu T. J., Ting C. T., Karagueuzian H. S., Garfinkel A., Lin S. F., Weiss J. N. (2003): A tale of two fibrillations. *Circulation* **108**, 2298—2303
- Clayton R. H., Parkinson K., Holden A. V. (2002): Re-entry in computer models of ischaemic myocardium. *Chaos Soliton Fractals* **13**, 1671—1683
- Fast V. G., Pertsov A. M. (1992): Shift and termination of functional reentry in isolated ventricular preparations with quinidine-induced inhomogeneity in refractory period. *J. Cardiovasc. Electrophysiol.* **3**, 255—265
- Irisawa H., Sato R. (1986): Intra- and extracellular actions of proton on the calcium current of isolated guinea pig ventricular cells. *Circ. Res.* **59**, 348—355
- Janse M. J. (1992): The premature beat. *Cardiovasc. Res.* **26**, 89—100
- Jin Y. B., Yang L., Zhang H., Kuo Y. H., Huang Y. Z., Jiang D. Z. (2004): Numerical algorithm for conduction of action potential in two-dimensional cardiac ventricular tissue. *Journal of Xi'an Jiaotong University* **38**, 851—854 (in Chinese)
- Luo C. H., Rudy Y. (1991): A model of the ventricular cardiac action potential. Depolarization, repolarization, and their interaction. *Circ. Res.* **68**, 1501—1523
- Luo C. H., Rudy Y. (1994): A dynamic model of the cardiac ventricular action potential. I. Simulations of ionic currents and concentration changes. *Circ. Res.* **74**, 1071—1096
- Noble D., Noble S. J., Bett G. C. L. (1991): The role of sodium-calcium exchange during the cardiac action potential. *Ann. N. Y. Acad. Sci.* **639**, 334—353
- Noble D., Varghese A., Kohl P., Noble P. (1998): Improved guinea-pig ventricular cell model incorporating a diadic space, I_{Kr} and I_{Ks} , and length- and tension-dependent processes. *Can. J. Cardiol.* **14**, 123—134
- Noma A. (1983): ATP-regulated K^+ channels in cardiac muscle. *Nature* **305**, 147—149
- Qu Z., Garfinkel A. (1999): An advanced algorithm for solving partial differential equation in cardiac conduction. *IEEE Trans. Biomed. Eng.* **46**, 1166—1168
- Qu Z., Weiss J. N., Garfinkel A. (1999): Cardiac electrical restitution properties and the stability of reentrant spiral waves: a simulation study. *Am. J. Physiol.* **276**, 269—283
- Qu Z., Xie F. G., Garfinkel A., Weiss J. N. (2000): Origins of spiral wave meander and breakup in a two-dimensional cardiac tissue model. *Ann. Biomed. Eng.* **28**, 755—771
- Shaw R. M., Rudy Y. (1997a): Electrophysiologic effects of acute myocardial ischemia: a theoretical study of altered cell excitability and action potential duration. *Cardiovasc. Res.* **35**, 256—272

- Shaw R. M., Rudy Y. (1997b): Electrophysiologic effects of acute myocardial ischemia: a mechanistic investigation of action potential conduction and conduction failure. *Circ. Res.* **80**, 124—138
- Starmer C. F., Romashko D. N., Reddy R. S. (1995): Proarrhythmic response to potassium channel blockade: numerical studies of polymorphic tachyarrhythmias. *Circulation* **92**, 595—605
- Taggart P., Sutton M. I., Boyett M. R. (1996): Human ventricular action potential duration during short and long cycles-rapid modulation by ischemia. *Circulation* **94**, 2526—2534
- Tsunetoyo N., Takashi A., Kazuo N., Tohru O. (2000): Spatial heterogeneity in refractoriness as a proarrhythmic substrate – theoretical evaluation by numerical simulation. *Jpn. Circ. J.* **64**, 121—129
- Viswanathan P. C., Shaw R. M., Rudy Y. (1999): Effect of *I_{Kr}* and *I_{Ks}* heterogeneity on action potential duration and its rate dependence. *Circulation* **99**, 2466—2485
- Wu T. J., Lin S. F. (2002): Two types of VF in isolated rabbit hearts: importance of excitability and action potential duration restitution. *Circulation* **106**, 1859—1866
- Winfree A. T. (1994): Electrical turbulence in three-dimensional heart muscle. *Science* **222**, 1003—1006
- Xie F. G., Qu Z. L., Garfinkel A., Weiss J. N. (2001): Effects of simulated ischemia on spiral wave stability. *Am. J. Physiol., Heart. Circ. Physiol.* **280**, H1667—1673

Final version accepted: August 8, 2005